Review

A Review on the Use of Biochar Derived Carbon Quantum Dots Production for Sensing Applications

Giovanni Lo Bello [1], Mattia Bartoli [2,3,*], Mauro Giorcelli [1,3], Massimo Rovere [1,3] and Alberto Tagliaferro [1,3,*]

1   Department of Applied Science and Technology, Politecnico di Torino, 10129 Turin, Italy;
    giovanni.lobello97@gmail.com (G.L.B.); mauro.giorcelli@polito.it (M.G.); massimo.rovere@polito.it (M.R.)
2   Center for Sustainable Future Technologies, Italian Institute of Technology, Via Livorno 60, 10129 Turin, Italy
3   Consorzio Interuniversitario Nazionale per la Scienza e Tecnologia dei Materiali (INSTM),
    10144 Florence, Italy
*   Correspondence: mattia.bartoli@polito.it (M.B.); alberto.tagliaferro@polito.it (A.T.);
    Tel.: +39-0110907346 (M.B.); +39-0110907338 (A.T.)

Abstract: Since their discovery, carbon dots have attracted a great deal of interest for their perspective biological applications. Nevertheless, the quenching of carbon dots photoluminescence represents an interesting feature for quantitative analysis in very low concentration of many species. A particular approach for the production of carbon dots is the use of biochar, a carbonized biomass, as a precursor. In this work, we overview the main achievements accomplished by using biochar-derived carbon dots for detecting and quantifying inorganic and organic species. We also provide background knowledge of the main properties, production and purification routes of carbon dots.

Keywords: biochar; carbon quantum dots; chemical sensing

1. Introduction

Biochar (BC) is a carbon material recovered from the conversion of biomasses under high temperature in a poorly or non-oxidative atmosphere [1]. BC is commonly used in environmental remediation [2] and as soil amelioration [3]. Nevertheless, BC has yet to experience a real breakthrough. Maroušek et al. [4] sharply pointed out the failure of BC use in land carbon sequestrations, as the high cost prevents massive use of BC as an agricultural amendment. This unneglectable issue becomes marginal if BC is used for high cost applications such as energy storage [5,6], as a flame retardant additive [7–9], a conductive filler for improving mechanical and electrical properties of both a polymeric [10–17] and cement matrix [18–21], and as a catalyst [22].

Nowadays, BC has been considered in many fields, but there is still a search for so-called "killer applications" that will make it the carbon material for a sustainable world.

A good chance is represented by the conversion of pristine BC into nanostructured materials with superior electric performances. For this purpose, Carbon Dots (CDs) have gained great attention as the newest carbon-based nanomaterials.

CDs are a class of fluorescent carbon-based nanomaterials discovered by chance in 2004, when Xu et al. [23] tried to purify single-walled carbon nanotubes. CDs have been shown to be a valid alternative to Quantum Dots (QDs) thanks to their simple preparation methods and multiple inherent properties such as intrinsic biocompatibility, water solubility, chemical inertness, and photoluminescence [24]. This wide spectrum of properties allows them to be used both in diagnostic and therapeutic fields, for example as a vehicle for drug release, as probe molecules (thanks to their excellent fluorescence properties), or for bioimaging and biosensing techniques [25–27].

Over the years, many hypotheses have been made about CD structure [28]. Of note, CDs are very different according to the various precursors used and preparation routes

followed. Nevertheless, several authors have proposed a general model for CDs with an inner graphitic core with amorphous region close to the edges [29]. Others have suggested interpretative models based on an amorphous core [30]. The more reliable classification based on the structure was reported by Mintz et al. [31], who classified three great families of CDs: (i) graphitic, (ii) nitride based, and (iii) polymeric ones. Each group displayed peculiar characteristics and chemical signatures. Graphitic CDs have attracted the greatest interest due to their tremendous versatility and similarity to graphene derivatives. Graphene CDs have proved to be a very powerful species for chemical sensing and bioimaging [32,33].

However, the synthesis of these nanomaterials requires considerable energy consumption and a chemical oxidation step which is performed in environmental unfriendly conditions [34]. Accordingly, research has investigated new productive routes based on environmentally sustainable materials for the production of high performance CDs for sensing uses.

In this review, we try to provide an overview, updated at the end of 2021, of the research concerning the use of BC for the production of CDs and of their applications in chemical sensing, providing a comprehensive overview of inorganic and organic species detection.

2. Carbonization of Biomass: From BC to BCCDs

2.1. BC Production

As stated above, BC is produced through thermochemical cracking of biomasses under different conditions. The main routes for biochar production are torrefaction, hydrothermal liquefaction, pyrolysis, and gasification. The main and more relevant difference between these routes is represented by the different temperature and reaction medium used.

During torrefaction, process temperature can reach up to 200–350 °C, achieving only a partial carbonization of biomass [35]. BC produced from biomass torrefaction displays a carbon content of up to around 50 wt.% with yields of up to 70% [36], but can reach values close to 80 wt.% through the use of microwave assisted processes [37–41].

Under pyrolytic conditions, process temperature is increased above 400 °C, promoting advanced cracking reactions in an oxygen-free atmosphere with yields of BC ranging from 30 wt.% up 50 wt.% [42].

Contrary to pyrolysis, gasification occurs in an oxidant atmosphere such as air [43], oxygen, or steam [44] at temperatures higher than 800 °C with or without the addition of a catalyst [45]. The main gasification output is represented by gas, but BC is also produced in a low amount and with high ash content [46].

Hydrothermal liquefaction (HTC) is a different route compared to the previous ones because it is run in a water medium at low temperatures ranging from 140 °C up to 380 °C under pressure in the range of 4 atm up to 220 atm [47]. The hydrothermal liquefaction process is far less efficient than the other for BC production, with maximum yields of up to around 15 wt.%. Nevertheless, BC produced using this last approach shows a very high surface area and a great amount of polar functionalities on its surface [48].

2.2. BCCDs Production

BCCDs production converts low-value biomass waste into valuable and useful materials. There are essentially two main methodologies for the synthesis of BCCDs: top-down and bottom-up methods. Top-down methods involve the cleavage of bigger carbon structures while bottom-up methods build up the structures from small precursors. Common methods for BCCDs production include HTC, microwave-hydrotermal, pyrolysis carbonization, etc.

HTC exploits temperature (180–380 °C) and pressure for a few hours to convert BC in BCCDs for a wide variety of applications [49]. Microwave-hydrothermal method uses microwaves to heat water, an approach not commonly used, yet it allows for obtaining narrow and uniform size distribution (generally between 1 and 5 nm) [50]. Pyrolysis is one of the common methods for BCCDs production and involves the decomposition of

a carbon source by heat. Also, in this case, the as-prepared BCCDs show a narrow size distribution ranging from 0.4 to 2.0 nm [51].

There are many studies that describe BCCDs production exploiting simple heating of organic molecules such as urea, aromatic amine, or organic acids [52]. This approach involves different stages, including dehydration, polymerization carbonization, and passivation [53].

Many authors have observed that higher reaction temperatures influence particle size and QY value. In particular, the higher the reaction temperature (up to 180 °C under hydrothermal conditions), the lower the particle size (down to 3 nm) [54].

The unique combination of spectroscopic and morphological features of carbon dots, as shown in Figure 1 according Mintz [31], represent the most characteristic properties of CDs.
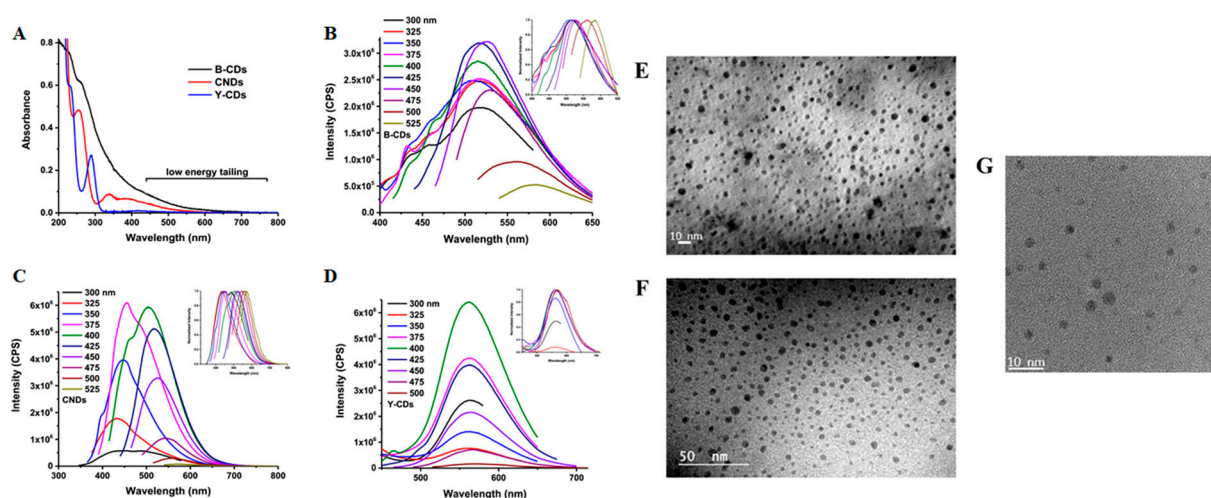

Figure 1. UV-Vis (**A**), fluorescence (**B**–**D**) and TEM (**E**–**G**) of three CDs produced from carbon soot (B-CDs), from citric acid and urea (CNDs), and from citric acid and 1,2-diaminebenzene as reported by Mintz [31]. Reprint with all permissions from Elsevier.

Other studies have shown how a low-temperature carbonization and simple filtration can be used to synthesize BCCDs. The as-prepared CDs exhibited small particle sizes (down to 2 nm) and good stability in a wide range of pH values (2–11) [55].

As stated, HTC is the preferred thermochemical route for the production of BCCDs, but is not sufficient to produce pure materials. A key step for the recovery of BCCDs is the purification of BC precursor though dialysis, as shown in Figure 2.
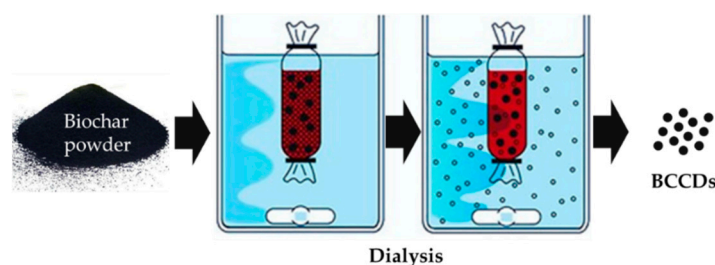
Figure 2. Dialysis purification of BC for the isolation of BCCDs.

Dialysis purification of suspended BC allows for cutting out particles of different molecular size, isolating them inside or outside the membrane. Dialytic procedure is the unavoidable stage for any CDs production, and could be coupled with other approaches such as a chromatographic one for further refining of the CDs size distribution [56,57].

Size distribution is strongly related to all the CDs features such as PL [58] and biological exploits [59].

3. BCCDs for Sensing Applications

3.1. BCCDs Properteis

CDs are carbon based nanomaterials with an average size of down to few nanometers regrouped in three main families: graphene-like, carbon nitride, and polymeric CDs [60].

The most relevant property of CDs is undoubtedly the photoluminescence (PL). PL of CDs is a complex phenomenon involving at least four different mechanisms [61]. The first is the quantum confinement effect due to the conjugated π-domains, which is related to the inner core structure of CDs [62]. The second effect is related to the put shell of CDs and is due to the hybridization of the carbon atoms backbones and to the residual functionalities [63]. The third one is the simplest and is due to fluorescent molecules entrapped and bonded to the CDs structures. The last one is the crosslink enhanced emission and it is characteristic of polymeric CDs [64].

Similar to graphene CDs, BCCDs exploit the first two mechanism mentioned due to their high carbon content. Yu et al. [65] comprehensively described the PL of graphene-like CDs by varying the core/shell ratio and surface functionality, hypothesizing an emission mechanism, as shown in Figure 3.
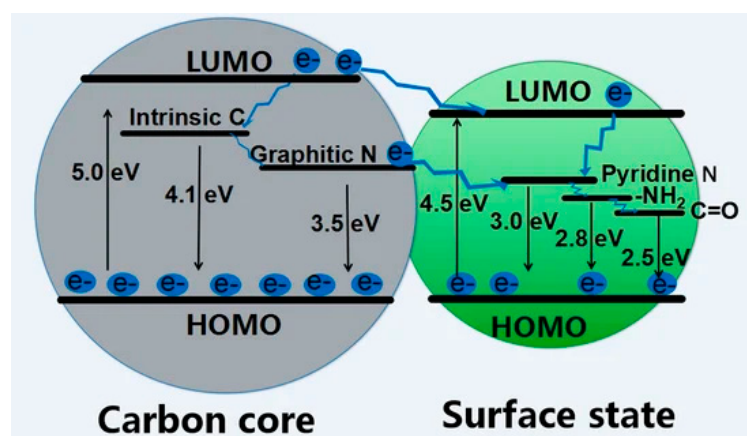

Figure 3. Scheme of the luminescence pathway and corresponding energy in graphene CDs with different core/shell ratio and surface functionalities. Reprinted with permission from [65] under CC BY 4.0.

PL is also the key for using CDs for chemical sensing due to the quenching phenomena occurring in the presence of metal ions [66,67]. Furthermore, the interaction between CDs and organic molecules could also alter PL emission [68].

The mechanisms laying behind PL quenching are numerous (static quenching [69], dynamic quenching [70], Förster resonance energy transfer [71], photoinduced electron transfer [72], surface energy transfer [73], Dexter energy transfer [74], inner filter effect [75]), and they are related to the interaction occurring between CDs and the quencher.

Static quenching is due to the formation of a ground state complex between CDs and a quenching agent, while the dynamic one occurs as a consequence of the diffusion process of a quenching agent while CDs is in its excited state [76].

Förster resonance energy transfer takes place between a quenching agent and CDs over great distances up to 10 nm, interacting mainly through dipole-dipole interaction [77]. Contrarily, a short scale interaction length is necessary for photoinduced electron transfer occurring with the association of CDs and a quenching agent on a sub-nanometric scale [78]. Surface energy transfer is more related to the quenching of inorganic dots as a consequence of the interaction of surface plasmons and a fluorophore [79], but could also occur during interactions between CDs and small metal clusters [80]. Dexter energy transfer takes place on the same scale length of Förster resonance energy transfer, but involves an orbital overlapping [81]. The inner filter effect has been considered an error in PL measurements,

but is a real phenomenon due to the overlap of the absorption spectrum of the quencher with the excitation or emission spectrum of CDs [82].

PL emission modification caused by external stimuli represent the pillar of use of CDs for a sensing application, as we discuss in the next sections.

Nevertheless, CDs derived from highly graphitic precursors could be also be used for electrochemical sensing [83].

3.2. BCCDs for Detection of Inorganic Species

Several studies have been devoted to the use of many BCs for the detection of metal ions [84]. Nevertheless, BCCDs represent a new approach in the field with unravelled potentialities, as summarized in Table 1.

Table 1. Summary of the main study on inorganic ions in water phase detection by using BCCDs materials.

Application	Production Route	Average Size (nm)	Quantum Yield (%)	Detection Limit (µM)	Linearity Range (µM)	Ref.
Fe(III) detection	• Hydrothermal conversion (180 °C) of domestic waste	15.3	28	0.0001	0.001–0.01	[85]
	• Hydrothermal conversion (160 °C) of wheat, rice and corn straw	2.5	3.5	5	5–500	[86]
	• Pyrolysis up to 400 °C of mango peel and oxidation with sulfuric acid	3.7	11.5	Not reported	4–200	[87]
	• Hydrothermal conversion (180 °C) of sweet potato and glycine	3.5	2.8	0.3	1–100	[88]
	• Hydrothermal conversion (200 °C) of orange peel, ginkgo biloba leaves, paulownia leaves and magnolia flower	2.6	8.1	0.08	0.2–100	[89]
	• Hydrothermal conversion (200 °C) of Lycii Fructus	3.3	17.2	0.02	1–30	[90]
	• Hydrothermal conversion (200 °C) of lignin	4.9	23.7	0.8	1–300	[91]
	• Hydrothermal conversion (200 °C) of waste rice and glycine	2.7	23.5	0.8	30–200	[92]
	• Hydrothermal conversion (150 °C) of wood waste	<10	28.3	32	150–500	[93]
	• Hydrothermal conversion (180 °C) of fruit extract	5	8.7	70	125–500	[94]
	• Hydrothermal conversion (180 °C) of blue grass	8.5	7.3	1	5–25	[95]

<div align="center">**Table 1.** *Cont.*</div>

Application	Production Route	Average Size (nm)	Quantum Yield (%)	Detection Limit (µM)	Linearity Range (µM)	Ref.
Cu(II) detection	. Hydrothermal conversion (200 °C) of bamboo leaves and amines	3.6	7	0.1	1–140	[96]
	. Microwave carbonization of mushroom 800 W	2.6	7.6	0.004	0.01–500	[97]
	. Microwave carbonization of fruit bunch 800 W			0.4	1–400	[98]
	. Peroxidation and hydrothermal conversion (200 °C) of prawn shells	7.6	12.3	0.005	0.010–1.1	[99]
Al(III) detection	. Hydrothermal conversion (160 °C) of Pyrus pyrifolia	2	10.8	0.003	0.005–100	[100]
	. Hydrothermal conversion (180 °C) of algae	68	10.2	<0.001	0.2–70	[101]
CrO_4^{2-} detection	. In-flow hydrothermal conversion (450 °C) of glucose	4.5	0.3	0.002	1–500	[102]
Hg(II) detection	. Microwave carbonization of lotus root using 800 W	9.4	5.2	0.019	0.2–60	[103]
	. Hydrothermal conversion (200 °C) of orange juice and amines	3	31.7	Not reported	4–32	[104]
	. Hydrothermal conversion (160 °C) of Pineapple Leaf Fiber	4.6	Not reported	<0.001	0.2–60	[105]
	. Low temperature pyrolysis (300 °C) of pigeon feathers, egg and manure	4.2	33.5	0.001	0.12–1.66	[106]
Ag(I) detection	. Long time hydrothermal conversion (180 °C, 8 days) of bean pod and onion	6	7.6	0.037	0.1–25	[107]
	. Hydrothermal conversion (260 °C) of purple perilla	2.8	9	0.001	0.002–0.010	[108]
AsO_4^{3-}/AsO_3^{3-} detection	. Microwave carbonization of quince fruit using 800 W	4.9	8.6	0.02	0.2–2	[109]
Co(II) detection	. Microwave carbonization of kelp and mines using 800 W	3.7	23.5	0.4	1–200	[110]
Cs(I) detection	. Hydrothermal conversion (190 °C) of maple leaves	10	Not reported	0.02	0.1–100	[111]

Application	Production Route	Average Size (nm)	Quantum Yield (%)	Detection Limit (μM)	Linearity Range (μM)	Ref.
ClO^- detection	• Hydrothermal conversion (180 °C) of pepper	7	7.1	0.05	variable	[112]
S^{2-} detection	• Hydrothermal conversion (200 °C) of carrots	4.8	Not reported	0.06	0.1–8	[113]
F^- detection	• Ultrasound carbonization of sugarcane bagasse	12	27	Not reported	10–160	[114]

Evaluation of Fe(III) and Fe(II) is a key issue in any water stream due to the large use of iron salt as a flocculant agent in wastewater treatment facilities [115].

Das et al. [85] converted several waste biomass (rose petals, banana peel, coffee, and tea waste) through the hydrothermal process at 180 °C, producing green mitting BCCDs. Authors reported wide size distribution based on the different precursors used from 7.2 nm using rose petals of up to 15.3 nm using spent coffee grounds. Through an optical approach, authors reported a range of quantification of Fe (III) in water from 1 nM up to 100 nM. Similar results were achieved for the detection of Cr (VI) ions. Interestingly, authors described an on-off behavior of the BCCDs after the addition of the metal ions solution, as reported in Figure 4.

Figure 4. Fluoresce quenching of blue emitting BCCDs in the presence of Fe(III) ions reported in [85]. Reprinted with permission from Elsevier.

Very similar behavior was observed for low temperature produced BCCDs reported by Şenol et al. [116]. Authors suggested that the on-off behavior was due to the formation of a non-radiative complex between Fe(III) and surface groups of BCCDs. Furthermore, authors observed the same trends in the presence of strong oxidant agents such as hypochloride ions able to oxidize the hydroxyl functionalities. Accordingly, they concluded that the presence of hydroxyl residues represent a must-have condition for iron sensing.

Ding and co-workers [86] used wheat, corn, and rice straw for the realization of blue emitting BCCDs with an optimal excitation wavelength in the range from 350 nm up to 390 nm. Authors pointed out that the emission was due to the transitions $\pi^* \rightarrow \pi$ of C=C and $\pi^* \rightarrow n$ of C=O. The sensitivity of the BCCDs was not so high, but still interestingly reached a detection limit of up to 5.23 μM for Fe(III) in a watery solution. Similar results were reported by Jiao et al. [87] by using mango peel as a BC precursor. Authors used pyrolytic conditions (400 °C of processing temperature in a nitrogen atmosphere), together with an oxidative process with sulfuric acid producing BCCDs with and average size in a range of 2 nm up to 6 nm and a quantum yield of 8.5 ± 0.2%. BCCDs emission was stable both in acidic and basic environment media, reaching a detection limit of Fe(III) up to 5 μM. Improved results on Fe ions detection were achieved by Shen et al. [88] using sweet potato under hydrothermal conditions for the production of hydroxyl rich BCCDs with a maximum emission at 440 nm. Authors claimed a limit of detection for of Fe(III) up to 0.3 μM.

Wang et al. [89] produced well-performing BCCDs using various exotic biomass with high water solubility and stability in wide pH and temperature ranges. The PL quenching

induced by the presence of Fe(III) led to a very low limit of detection of up to 0.08 μM. Similar results were achieved by using Lycii Fructus [90] and lignin [91].

Varying the BC precursor is not the only way to improve the iron detection performance of BCCDs. A very effective way to produce more performing materials is represented by heteroatom doping.

Qi et al. [92] produced nitrogen doped BCCDs using rice waste and glycine, achieving materials with a quantum yield of up to 24% and a maximum emission of up to 440 nm. Authors reported a low Fe(III) detection limit of up to 0.7 μM. Ahn et al. [93] produced BBCDs with blue emission and a quantum yield of 23%. Blue emitting BCCDs showed a higher detection limit of up to 32 μM but they were able to detect Fe(III) also in in vivo systems. Atchudan et al. [94] converted Chionanthus retusus fruit extract using a hydrothermal carbonization method operating at 180 °C for 6 h. The nitrogen-rich precursor led to the formation of nitrogen doped BCCDs with amine, pyridine, and pyrrole functions on the shell and an average size of up to 5 nm with an interlayer distance of 0.21 nm. Authors demonstrated a highly durable fluorescence with a quantum yield of 9% for the as-synthesized materials and a detection limit of 70 μM in vivo for Fe(III) detection.

Krishnaiah et al. [95] converted blue grass though hydrothermal routes at 180 °C for 36 h, producing nitrogen doped BCCDs. Authors observed fluorescence with a significant redshift from 370 to 470 nm using wavelengths ranging from 280 up to 400 nm, as shown in Figure 5.
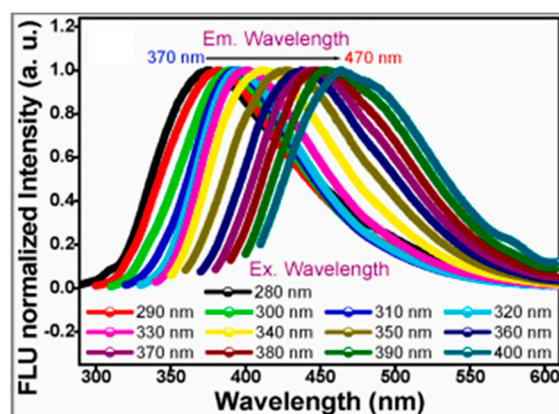

Figure 5. Red shift of green emitting BCCDs as reported in [95]. Reprinted with all permissions from Elsevier.

Excitation dependent emission represents a crucial issue in the understanding of CDs emission and is debated by several authors [117,118]. Authors suggest that this phenomenon was due to $n \rightarrow \pi^*$ transition occurring through non-bonding electrons of carbonyl and carboxylic groups of BCCDs outer shell. This behavior was in agreement with a structural study reported by Mintz et al. [31] and was reasonably affected by nitrogen atom inclusion. Authors also reported a quite low quantum yield of up to 7% and a high hydrophilicity, allowing the detection of both Fe(III) and Mn(III) ions in water medium. Authors reached a detection limit of up to 1.4 μM and a linearity range from 5 up to 25 μM. Furthermore, authors proved the stability of BCCDs in water solution evaluating the emission spectra of BCCDs in a 100-day period without observing any appreciable change. Nevertheless, these materials showed an appreciable loss of selectivity in the presence of Cd(III) and Pb(III).

Detection of Cu(III) is also a relevant task for water and biological applications due to the harmful potential for marine ecosystems [119,120] and the human body [121].

BCCDs are solid solutions to evaluate the copper cations concentration in watery medium due to the strong PL quenching induced by the Cu(III).

Liu et al. [96] produced a blue emitting BCCDs through the conversion of bamboo leaves and diamines at 200 °C for 6 h. The resulting BCCDs showed a maximum emission at

450 nm and a very low detection limit for Cu(III) in water media up to 115 nM. Furthermore, authors reported a remarkably selective quenching induced by Cu(III) over other metals (i.e., Co(III), Ca(III), Ni(III), Mn(III), Hg(III), Pb(III), Ba(III), and Cd(III)) while cations such as Fe(III) and Hg(III) appreciably interfered.

Bhamore et al. [97] used a microwave-assisted carbonization procedure for the conversion of seeds into 2.5 nm sized BCCDs. Authors used a monomodal microwave oven with a power of up to 800 W for 2 min and isolated the purified BCCDs through dialytic methods. The resulting BCCDs acted as "turn-off" sensors with an emission maximum at 468 for Cu(III) reaching a limit of detection of 4.3 nM. Furthermore, authors did not observe PL quenching in the presence of other metal cations, suggesting the production of a highly selective probe for Cu(III). Kamarol Zaman et al. [98] also produced blue emitting BCCds using microwave-assisted route and empty fruit bunch. BCCDs produced showed an emission peak at around 420 nm under UV irradiation. Authors reported a good detection limit for Cu(III) of up to 0.42 μM.

Gedda et al. [99] pre-oxidized prawn shells and hydrothermally converted them into blue emitted BCCDs with an average diameter of up to 4 nm and emission peaked at 390 nm under UV irradiation. As shown in Figure 6, the selectivity of these species for Cu(III) was also quite good in real marine water samples.
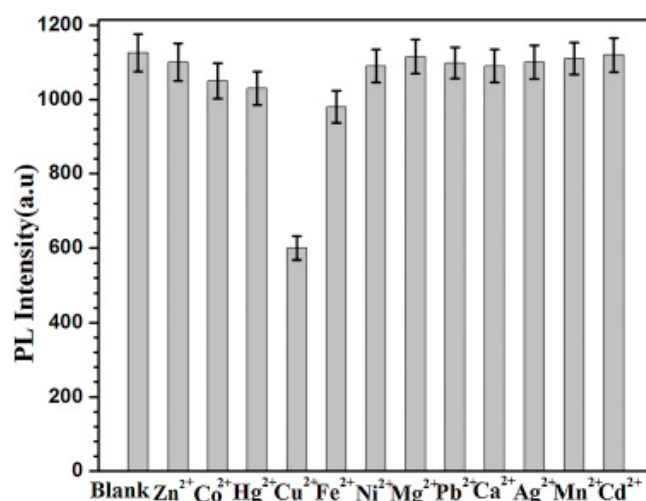

Figure 6. PL quenching reported by Gedda et al. [99] in presence of different metal ions with a concentratin of up to 5 μM. Picture reprinted with all permissions from Elsevier.

Authors suggested that the selectivity observed was due to the specific quenching mechanism related to the interaction between Cu(III) and amine residue with the formation of cupric amine acting specific UV/visible absorption.

Aluminum ions are another species that could represent a serious threat to human health [122]. Accordingly, Al(III) monitoring is also very relevant, and the use of low detection limit analytical routes is of great interest.

Accordingly, Bhamore and co-workers [100] developed an analytical route for Al(III) detection by using BCCDs produced from the hydrothermal conversion of waste pears. The blue emitting BCCDs showed a peak of emission close to 470 nm under UV irradiation and a size of up to around 2 nm. Authors reported a very low detection limit of 2.5 nM and a great selectivity to Al(III) in the presence of cations, anions, and organic species. This was justified by the selective formation of stable Al(III) chelated species on the outer shell of BCCDs that induced an irreversible quenching of PL. Similarly, Rao et al. [101] synthesized a dual emission BCCDs through the conversion of several algae under hydrothermal conditions at 180 °C for 10 h. The produced BCCDs showed two emissions peaked at 470 nm and 670 nm under a single excitation. Interestingly, the emission at 470 nm was selectively quenched by Al(III) even in the presence of other ions, while the one at 670 nm

was quenched by water. These BCCDs have been proposed as reliable chemosensors for both Al(III) and water evaluation in commercial fruit juices.

Baragau et al. [102] faced the issue of Cr(VI) detection by using BCCDs. Authors proposed an innovative in-flow hydrothermal route operating at 450 °C and with a constant pressure of up to 24.8 MP. BCCDs produced displayed a size of up to 2.3 nm, with an emission peaking at 446 nm on excitation at 360 nm. Authors claimed a limit of detection for Cr (VI) of up to 2 μM. Authors also reported the possibility of using the same BCCDs for Fe(III), but they did not evaluate the completion between the two inorganic species.

Another metal cation detectable by using PL quenching of BCCDs is Hg(III). Hg(III) is among the most toxic metal ions, having dramatic effects on human health [123]. Accordingly, Gu et al. [103] developed BCCDs from microwave carbonization of lotus root for detection of Hg(III) in water. The BCCDs synthesized showed a high content of nitrogen up to around 5% and a diameter close to 10 nm. Nevertheless, they were able to not only detect Hg(III) with a detection limit of 17 nM, but also to selectively capture the mercury ions without releasing them. These properties also allowed BCCDs to be used for environmental remediation purposes. Nitrogen doping is an essential feature for Hg(III) sensing though BCCds, as proved by many authors [104,105]. The abundance of nitrogen is directly related to the presence of amine and pyridine residues that boosted the capture of Hg(III) with an enhancement of PL quenching. The most effective BCCDs doping is represented by the simultaneous insertion of nitrogen and sulfur atoms, as mentioned by Ye et al. [106]. Authors co-pyrolysed pigeon feathers, egg, and manure and purified BCCDs through dialysis. The recovered materials showed a blue emission centered at 475 nm and an average size of up to 4 nm. The presence of sulfur atoms mainly included in the graphitic structures promoted the formation of stable bonds with Hg(III), reaching a detection limit of up to 10 nM.

The very same approach was used by Lu et al. [107] by hydrothermal treating bean pod and onion for 8 days at 180 °C for the detection of Ag(I). The blue emitting BCCDs reached a limit of detection OF 37 nM, showing the best nitrogen/sulfur ratio to be close to 3. Even better results were achieved by Zhao et al. [108]. Authors hydrothermally treated purple perilla at 260 °C after sonication in water medium, producing BCCDs with the astonishing detection limit of Ag(I) up to 1.4 nM. Similar results were achieved in the detection of As(III) [109] and Co(III) [110] by using microwave-assisted synthetic strategies.

Interestingly, Boruah et al. [114] reported an ultrasound-induced carbonization of biomass for the production of BCCDs able to detect fluoride ions. Authors converted sugar cane bagasse into blue emitting BCCDs that after doping with Eu(III) could be used for detecting fluoride down to a concentration of 10 μM.

Chellasamy et al. [111] converted maple leaves by using hydrothermal treatment at 190 °C for 8 h producing blue emitting BCCDs. Authors reported the formation of small BCCDs with an average size of up to 1–2 nm with a carbon structure quite ordered, as proved by the analysis of Raman spectra. Authors used the prepared materials for cesium detection in water media achieving a linearity range from 0.1 up to 100 μM and a detection limit of up to 0.16 μM without observing any appreciable interference effects from other ions. Interestingly, authors observed an appreciable modification of Raman spectra.

Yin et al. [112] developed BCCDs with symmetric emission spectra, large stock shifts, improved resistance to photobleaching, and excitation dependent emission. Curiously, authors reported a two-emission spectra with one emission peak centered at around 280 nm under UV irradiation and another one in the range from 450 m up to 600 nm under visible light. They suggest that this behavior was due to two different mechanisms; one due to to n → π* active in UV region and the other due to several structural factors (i.e., particle sizes distribution, different emissive centers, multiphoton processes). These two emission phenomena led to two linear ranges, one from 0.1 up to 10 μM, and one from 10 up top 300 μM. Authors achieved a very promising result in hypochloride detection in real water samples with percentage errors of around 2%.

Jin et al. [113] produced BCCDs conjugated with polyethyleneimine and nile blue for direct sensing of sulfide anions. Authors realized the chemical probe by assembling the

additive and BCCDs through supramolecular electrostatic interactions. Authors quenched the emission of BCCDs via inner filter effe by adding Cu(III) and using the non emitting BCCds adduct for the detection of sulfide. Sulfide species were able to tightly bond with copper ions and were removed from BCCDs, increasing the emission. Accordingly, this was one of the first studies reporting an off-to-on behavior of BCCDs in sensing applications. Authors reached the interesting detection limit of 0.06 μM with a linearity range from 0.1 up to 8.0 μM.

Other BCCDs systems were able to detect more than one heavy metal but not simultaneously [95,124] due to the coordination of metals on their outer shell.

Nevertheless, BCCDs uses are not limited to the detection of a single species, but could be used to assemble chemical platforms able to simultaneously detect multiple species. As reported by Fu and co-workers [125], waste animal bones could be converted through hydrothermal processes into BCCDs. These materials have been used to build a multi-channel array able to quantify and discriminate up to five different metal ions by modulating the PL emission. Authors claimed an accuracy up to 100% for individual, binary and ternary mixture of Ag (I), Cu(III), Hg(III), Fe(III) and Pb(III). Similarly, Plácido et al. [126] converted microalgae BC into BCCs producing a transducer for detecting Pb(III), Cu(III), Cd(III), and Ni(III) with good stability under a wide range of pH and resistant to photo-bleaching. Authors reported good detection limits ranging from 12 nM to 2 mM with an enhancement of detectability using slightly basic pH.

3.3. BCCDs for Detection of Organic Species

PL quenching of BCCDs is not limited to the interaction with inorganic species, but could also be induced by probe molecules [127], as summarized in Table 2.

Table 2. Summary of the main study on organic detection by using BCCDs materials.

Applications		Production Route	Size (nm)	Quantum Yield (%)	Detection Limit (μM)	Linearity Range (μM)	Ref.
Sensing of prilocaine	•	Hydrothermal conversion (200 °C) of saffron	7.5	23.6	1.8	0.003–0.400	[128]
Sensing of dimethoate	•	Pyrolysis (700 °C) of food waste	4.2	Not reported	0.06	0.15–5	[129]
Sensing of imatinib	•	Hydrothermal conversion (180 °C) of starch	Not reported	Not reported	0.002	10–400	[130]
Sensing of glyphosate	•	Hydrothermal conversion (200 °C) of wool	2.8	16.3	0.012	0.025–25	[131]
Sensing of biothiols	•	Hydrothermal conversion (200 °C) of silkworms' excrements	62	13.1	0.2	1–1000	[132]
Sensing of ascorbic acid	•	Hydrothermal conversion (180 °C) of milk powder in the presence of $FeCl_3$	2.9	8.7	9	20–500	[133]
Sensing phoxim	•	Hydrothermal conversion (180 °C) of Lycii Fructus			0.04	0.1–100	[134]
Sensing of baicalin	•	Low temperature carbonization (200 °C) of grape peels mixed with urea	7	Not reported	0.04	0.1–20	[135]

Table 2. *Cont.*

Applications		Production Route	Size (nm)	Quantum Yield (%)	Detection Limit (µM)	Linearity Range (µM)	Ref.
Sensing of tetracyclines	.	Hydrothermal conversion (200 °C) of waste tobacco	6.3	13.7	0.05	1–120	[136]
	.	Hydrothermal conversion (200 °C) of sweet potato peel	31	8.9	0.015	0.025–1	[137]
	.	Hydrothermal conversion (200 °C) of waste rice	2.7	23.5	0.24	1–250	[92]
	.	Hydrothermal conversion (200 °C) of tobacco	2.1	27.9	0.01	0.04–6	[138]
	.	Hydrothermal conversion (200 °C) of carp roe	7.6	13.4	0.04	0.1–50	[139]

Ensafi et al. [128] synthesized BCCDs from saffron by hydrothermal treatment for sensing of prilocaine. BCCDs showed a quantum yield of up to 24 and a size lower than 10 nm with an emission peaking at 460 nm. Authors reported a very interesting detection limit of prilocaine in water medium of up to 1.8 nM that was better than results achievable with LC-MS and comparable with GC–MS–electron impact ionization selected ion monitoring techniques. Furthermore, BCCDs were highly selective in real blood medium, as shown in Figure 7.
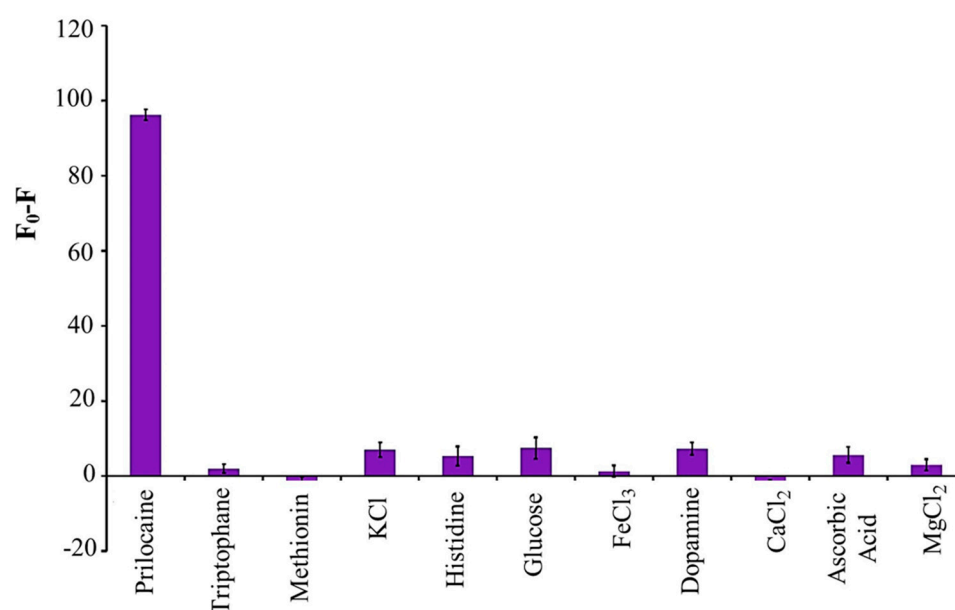
Figure 7. Selectivity calculated as differences between neat and conjugated of the BCCDs reported in [128] for prilocaine in real human blood at pH 4. Picture reprinted with all permissions from Elsevier.

Liu et al. [129] pyrolyzed pork ribs at 700 °C, producing BCCDs of 3–4 nm size with an emission peaked at 453. Authors used BCCDs for detection of dimethoate, finding a detection limit of 64 nM at pH 11 in water medium. A similar strategy was used by Yan et al. [130] for the detection of imatinib. Authors reached a detection limit of up to 2 nM as a consequence of a strong charge transfer quenching phenomenon. Wang et al. [131] hydrothermal converted waste wool at 200 °C, producing BCCDs with a 480 nm emis-

sion under UV irradiation. Authors combined this material with silver nanoparticles for glyphosate detection in water medium, reaching a detection limit of up to 12 nM.

Lu et al. [132] approached the sensing of biothiols by synthesizing BCCDs from excrements of silk worms and quenched their fluorescence emission by adding Fe(III). The non-emitting BCCDs were able to detect the presence of thiols containing species due to the ability of the iron sites to form stable complex bonding thiols functions. This behavior was detrimental for quenching phenomena and allowed for detecting cysteine and glutathione with detection limits close to 4 μM.

Tang et al. [135] carbonized grape peels mixed with urea at a low temperature (200 °C) to produce highly nitrogen-doped BCCDs for flavonoid detection. Their simple solid approach paved the way to easily-scalable nitrogen doped BCCDs production able to achieve detection limits approaching 0.05 μM.

Fan et al. [133] used a very close approach to detect ascorbic acid. Authors directly prepared blue emitting BCCDs through the conversion of milk powder mixed with iron chloride using hydrothermal treatment. The iron-containing BCCDs were able to oxidize 3,3′,5,5′-tetramethylbenzidine and quenched themselves. The quenched BCCDs were able to detect ascorbic acid to a reductive process that remove 3,3′,5,5′-tetramethylbenzidine from the BCCDs, restoring the fluorescence emission and reaching a detection limit of up to 5.3 μM.

Zheng et al. [134] used BCCDs derived from Lycii Fructus mixed with silver nanoparticles for the detection of phoxim with a linearity range from 0.1–100 μM and a detection limit of up to 0.04 μM. Authors described with good detail the mechanism of detection based on complex interactions between BCCds functions, nanoparticles, and analyte. The mechanism is based on a first interaction between silver nanoparticles and amino groups on the outer shell of BCCDs through electrostatic forces. By using a slightly acid pH, the cyano and ethoxy functions of phoxim carried positive charges and can interact with negative charges on the surface of BCCDs adducts forming a complex interactive network. This allows us to extend the detection close to the one achievable with the HPLC-MS technique.

Several studies have been focused on the detection of a particular class of antibiotics represented by tetracyclines. Tetracyclines are of paramount of importance due to their diffuse use and classification as emerging water pollutants [140].

Accordingly, Liang et al. [136] converted waste tobacco into BCCDs and used them to detect tetracyclines in water. Authors reached a detection limit of up to 1.5 μM and an accuracy for sample in the range of 30 μM to 60 μM, equal to that achieved by using HPLC quantifications.

Liu et al. [137] used sweet potato as a precursor for oxytetracycline determination with a detection limit of up to 0.013 μM that is even better than the commonly achieved one [141]. Other approaches used nitrogen doping [92] for further boosting of the BCCDs ability to detect tetracyclines in watery medium, outperforming chromatographic methods.

Miao et al. [138] converted tobacco leaves for the detection of three kinds of tetracyclines, proposing a detection mechanism based on two different effects related to surface defects and to quantum size of BCCDs. Authors produced a simple paper-based device able to visually discriminate tetracyclines from compounds such as cysteine and rose Bengal.

Furthermore, Tang et al. [139] proved the ability of BCCDs to detect tetracycline, chlortetracycline, and oxytetracycline in living cell human colon cancer cells and mouse cardiomyocytes, reaching detection limits of up to 0.05 μM. Similarly, Gunjal et al. [142] were able to detect tetracycline in urine and yeast cultivation media with a detection limit of up to 0.04 μM.

4. Challenges and Perspectives

The use of biomass for the production of CDs is very attractive due to the combination of sustainability goals and the great availability of feedstock. Nevertheless, the use of biomass reduced the synthetic tools for the researcher that is approaching BCCDs production. A common synthesis of CDs is far more tuneable [143] than one based on thermal

or hydrothermal conversion of biomass [144]. This issue could be overcome through a fine-tuning of production environment (i.e., temperature, heating rate, solvent, heating source) in order to use the biomass scaffolds to orientate the BCCDs towards nanostructure with appropriated size, functionalities, and quantum yield. Also, BCCDs represent the more solid bridge between graphene-like CDs and the other CDs families due to the tuneable graphitization obtained by modifying the production process. This could represent a valuable opportunity to produce fluorescence and proper electrochemical based sensors for a great variety of analytes [145]. The field of CDs based sensing is still open for big discoveries, and anarchy is ruling the research, but we firmly hope that the advance in comprehension of CDs structure-activity will lead to more goal-oriented research in the near future.

5. Conclusions

The use of CDs as molecular probes for the detection of inorganic and organic species is becoming a topic of paramount importance. Nevertheless, interest in the use of CDs outside the biological fields has attracted the attention of environmental issues related to the CDs production routes. BCCDs could represent a suitable solution combining the key features of CDs together with the reduced environmental footprint of BC. The positive BCCDs performances achieved for inorganic species detecting and quantification outperformed even the most accurate and sensible traditional methods such as chromatographic approaches.

Organic detection is far from being simultaneously qualitative and quantitative but BCCDs development has room for improvement.

Accordingly, we believe that BCCDs use for sensing will be one of the game changing approaches in analytical chemistry, moving us toward a major breakthrough in the scientific community.

Conflicts of Interest: The authors declare no conflict of interest.

References

1. Cha, J.S.; Park, S.H.; Jung, S.-C.; Ryu, C.; Jeon, J.-K.; Shin, M.-C.; Park, Y.-K. Production and utilization of biochar: A review. *J. Ind. Eng. Chem.* **2016**, *40*, 1–15. [CrossRef]
2. Beesley, L.; Moreno-Jiménez, E.; Gomez-Eyles, J.L.; Harris, E.; Robinson, B.; Sizmur, T. A review of biochars' potential role in the remediation, revegetation and restoration of contaminated soils. *Environ. Pollut.* **2011**, *159*, 3269–3282. [CrossRef]
3. El-Naggar, A.; Lee, S.S.; Rinklebe, J.; Farooq, M.; Song, H.; Sarmah, A.K.; Zimmerman, A.R.; Ahmad, M.; Shaheen, S.M.; Ok, Y.S. Biochar application to low fertility soils: A review of current status, and future prospects. *Geoderma* **2019**, *337*, 536–554. [CrossRef]
4. Maroušek, J.; Vochozka, M.; Plachý, J.; Žák, J. Glory and misery of biochar. *Clean Technol. Environ. Policy* **2017**, *19*, 311–317. [CrossRef]
5. Lee, H.W.; Kim, Y.-M.; Kim, S.; Ryu, C.; Park, S.H.; Park, Y.-K. Review of the use of activated biochar for energy and environmental applications. *Carbon Lett.* **2018**, *26*, 1–10.
6. Liu, W.-J.; Jiang, H.; Yu, H.-Q. Emerging applications of biochar-based materials for energy storage and conversion. *Energy Environ. Sci.* **2019**, *12*, 1751–1779. [CrossRef]
7. Barbalini, M.; Bartoli, M.; Tagliaferro, A.; Malucelli, G. Phytic Acid and Biochar: An Effective All Bio-Sourced Flame Retardant Formulation for Cotton Fabrics. *Polymers* **2020**, *12*, 811. [CrossRef] [PubMed]
8. Matta, S.; Bartoli, M.; Arrigo, R.; Frache, A.; Malucelli, G. Flame retardant potential of Tetra Pak®-derived biochar for ethylene-vinyl-acetate copolymers. *Compos. Part C Open Access* **2022**, *8*, 100252. [CrossRef]
9. Matta, S.; Bartoli, M.; Frache, A.; Malucelli, G. Investigation of Different Types of Biochar on the Thermal Stability and Fire Retardance of Ethylene-Vinyl Acetate Copolymers. *Polymers* **2021**, *13*, 1256. [CrossRef] [PubMed]
10. Arrigo, R.; Bartoli, M.; Malucelli, G. Poly (lactic Acid)–Biochar Biocomposites: Effect of Processing and Filler Content on Rheological, Thermal, and Mechanical Properties. *Polymers* **2020**, *12*, 892. [CrossRef] [PubMed]
11. Arrigo, R.; Jagdale, P.; Bartoli, M.; Tagliaferro, A.; Malucelli, G. Structure–Property Relationships in Polyethylene-Based Composites Filled with Biochar Derived from Waste Coffee Grounds. *Polymers* **2019**, *11*, 1336. [CrossRef] [PubMed]

12. Bartoli, M.; Giorcelli, M.; Rosso, C.; Rovere, M.; Jagdale, P.; Tagliaferro, A. Influence of Commercial Biochar Fillers on Brittle-ness/Ductility of Epoxy Resin Composites. *Appl. Sci.* **2019**, *9*, 3109. [CrossRef]

13. Bartoli, M.; Nasir, M.A.; Passaglia, E.; Spiniello, R.; Jagdale, P.; Rosso, C.; Giorcelli, M.; Rovere, M.; Tagliaferro, A. Influence of pyrolytic thermal history on olive pruning biochar and related epoxy composites mechanical properties. *J. Compos. Mater.* **2020**, *54*, 1863–1873. [CrossRef]

14. Giorcelli, M.; Bartoli, M. Development of Coffee Biochar Filler for the Production of Electrical Conductive Reinforced Plastic. *Polymers* **2019**, *11*, 1916. [CrossRef]

15. Giorcelli, M.; Bartoli, M.; Sanginario, A.; Padovano, E.; Rosso, C.; Rovere, M.; Tagliaferro, A. High-Temperature Annealed Biochar as a Conductive Filler for the Production of Piezoresistive Materials for Energy Conversion Application. *ACS Appl. Electron. Mater.* **2021**, *3*, 838–844. [CrossRef]

16. Noori, A.; Bartoli, M.; Frache, A.; Piatti, E.; Giorcelli, M.; Tagliaferro, A. Development of Pressure-Responsive PolyPropylene and Biochar-Based Materials. *Micromachines* **2020**, *11*, 339. [CrossRef]

17. Bartoli, M.; Torsello, D.; Piatti, E.; Giorcelli, M.; Sparavigna, A.C.; Rovere, M.; Ghigo, G.; Tagliaferro, A. Pressure-Responsive Conductive Poly(vinyl alcohol) Composites Containing Waste Cotton Fibers Biochar. *Micromachines* **2022**, *13*, 125. [CrossRef]

18. Gupta, S.; Kua, H.W.; Low, C.Y. Use of biochar as carbon sequestering additive in cement mortar. *Cem. Concr. Compos.* **2018**, *87*, 110–129. [CrossRef]

19. Wang, L.; Chen, L.; Tsang, D.C.; Guo, B.; Yang, J.; Shen, Z.; Hou, D.; Ok, Y.S.; Poon, C.S. Biochar as green additives in cement-based composites with carbon dioxide curing. *J. Clean. Prod.* **2020**, *258*, 120678. [CrossRef]

20. Gupta, S.; Kua, H.W. Effect of water entrainment by pre-soaked biochar particles on strength and permeability of cement mortar. *Constr. Build. Mater.* **2018**, *159*, 107–125. [CrossRef]

21. Gupta, S.; Muthukrishnan, S.; Kua, H.W. Comparing influence of inert biochar and silica rich biochar on cement mortar–Hydration kinetics and durability under chloride and sulfate environment. *Constr. Build. Mater.* **2021**, *268*, 121142. [CrossRef]

22. Tamborrino, V.; Costamagna, G.; Bartoli, M.; Rovere, M.; Jagdale, P.; Lavagna, L.; Ginepro, M.; Tagliaferro, A. Catalytic oxidative desulphurization of pyrolytic oils to fuels over different waste derived carbon-based catalysts. *Fuel* **2021**, *296*, 120693. [CrossRef]

23. Xu, X.; Ray, R.; Gu, Y.; Ploehn, H.J.; Gearheart, L.; Raker, K.; Scrivens, W.A. Electrophoretic analysis and purification of fluorescent single-walled carbon nanotube fragments. *J. Am. Chem. Soc.* **2004**, *126*, 12736–12737. [CrossRef]

24. Lim, S.Y.; Shen, W.; Gao, Z. Carbon quantum dots and their applications. *Chem. Soc. Rev.* **2015**, *44*, 362–381. [CrossRef]

25. Wang, Y.; Hu, A. Carbon quantum dots: Synthesis, properties and applications. *J. Mater. Chem. C* **2014**, *2*, 6921–6939. [CrossRef]

26. Lin, L.; Rong, M.; Luo, F.; Chen, D.; Wang, Y.; Chen, X. Luminescent graphene quantum dots as new fluorescent materials for environmental and biological applications. *TrAC Trends Anal. Chem.* **2014**, *54*, 83–102. [CrossRef]

27. Huang, S.; Li, W.; Han, P.; Zhou, X.; Cheng, J.; Wen, H.; Xue, W. Carbon quantum dots: Synthesis, properties, and sensing applications as a potential clinical analytical method. *Anal. Methods* **2019**, *11*, 2240–2258. [CrossRef]

28. Liu, M.L.; Chen, B.B.; Li, C.M.; Huang, C.Z. Carbon dots: Synthesis, formation mechanism, fluorescence origin and sensing applications. *Green Chem.* **2019**, *21*, 449–471. [CrossRef]

29. Kelarakis, A. From highly graphitic to amorphous carbon dots: A critical review. *MRS Energy Sustain.* **2014**, *1*, E2. [CrossRef]

30. Sun, Y.-P.; Zhou, B.; Lin, Y.; Wang, W.; Fernando, K.S.; Pathak, P.; Meziani, M.J.; Harruff, B.A.; Wang, X.; Wang, H. Quantum-sized carbon dots for bright and colorful photoluminescence. *J. Am. Chem. Soc.* **2006**, *128*, 7756–7757. [CrossRef]

31. Mintz, K.J.; Bartoli, M.; Rovere, M.; Zhou, Y.; Hettiarachchi, S.D.; Paudyal, S.; Chen, J.; Domena, J.B.; Liyanage, P.Y.; Sampson, R.; et al. A deep investigation into the structure of carbon dots. *Carbon* **2021**, *173*, 433–447. [CrossRef]

32. Xu, D.; Lin, Q.; Chang, H.T. Recent advances and sensing applications of carbon dots. *Small Methods* **2020**, *4*, 1900387. [CrossRef]

33. Sun, X.; Lei, Y. Fluorescent carbon dots and their sensing applications. *TrAC Trends Anal. Chem.* **2017**, *89*, 163–180. [CrossRef]

34. Zheng, X.T.; Ananthanarayanan, A.; Luo, K.Q.; Chen, P. Glowing graphene quantum dots and carbon dots: Properties, syntheses, and biological applications. *Small* **2015**, *11*, 1620–1636. [CrossRef]

35. Chen, W.-H.; Peng, J.; Bi, X.T. A state-of-the-art review of biomass torrefaction, densification and applications. *Renew. Sustain. Energy Rev.* **2015**, *44*, 847–866. [CrossRef]

36. Peng, J.; Bi, H.; Lim, C.; Sokhansanj, S. Study on density, hardness, and moisture uptake of torrefied wood pellets. *Energy Fuels* **2013**, *27*, 967–974. [CrossRef]

37. Undri, A.; Abou-Zaid, M.; Briens, C.; Berruti, F.; Rosi, L.; Bartoli, M.; Frediani, M.; Frediani, P. Bio-oil from pyrolysis of wood pellets using a microwave multimode oven and different microwave absorbers. *Fuel* **2015**, *153*, 464–482. [CrossRef]

38. Bartoli, M.; Rosi, L.; Giovannelli, A.; Frediani, P.; Frediani, M. Bio-oil from residues of short rotation coppice of poplar using a microwave assisted pyrolysis. *J. Anal. Appl. Pyrolysis* **2016**, *119*, 224–232. [CrossRef]

39. Bartoli, M.; Rosi, L.; Giovannelli, A.; Frediani, P.; Frediani, M. Production of bio-oils and bio-char from Arundo donax through microwave assisted pyrolysis in a multimode batch reactor. *J. Anal. Appl. Pyrolysis* **2016**, *122*, 479–489. [CrossRef]

40. Bartoli, M.; Rosi, L.; Giovannelli, A.; Frediani, P.; Frediani, M. Characterization of bio-oil and bio-char produced by low-temperature microwave-assisted pyrolysis of olive pruning residue using various absorbers. *Waste Manag. Res.* **2020**, *38*, 213–225. [CrossRef]

41. Bartoli, M.; Rosi, L.; Giovannelli, A.; Frediani, P.; Frediani, M. Pyrolysis of a-cellulose in a microwave multimode batch reactor. *J. Anal. Appl. Pyrolysis* **2016**, *120*, 284–296. [CrossRef]

42. Bridgwater, A.V. Review of fast pyrolysis of biomass and product upgrading. *Biomass Bioenergy* **2012**, *38*, 68–94. [CrossRef]

43. Guizani, C.; Sanz, F.E.; Salvador, S. Influence of temperature and particle size on the single and mixed atmosphere gasification of biomass char with H_2O and CO_2. *Fuel Process. Technol.* **2015**, *134*, 175–188. [CrossRef]
44. Barisano, D.; Canneto, G.; Nanna, F.; Alvino, E.; Pinto, G.; Villone, A.; Carnevale, M.; Valerio, V.; Battafarano, A.; Braccio, G. Steam/oxygen biomass gasification at pilot scale in an internally circulating bubbling fluidized bed reactor. *Fuel Process. Technol.* **2016**, *141*, 74–81. [CrossRef]
45. Cheah, S.; Jablonski, W.S.; Olstad, J.L.; Carpenter, D.L.; Barthelemy, K.D.; Robichaud, D.J.; Andrews, J.C.; Black, S.K.; Oddo, M.D.; Westover, T.L. Effects of thermal pretreatment and catalyst on biomass gasification efficiency and syngas composition. *Green Chem.* **2016**, *18*, 6291–6304. [CrossRef]
46. Zhao, H.; Li, Y.; Song, Q.; Liu, S.; Yan, J.; Wang, X.; Ma, Q.; Shu, X. Investigation on the physicochemical structure and gasification reactivity of nascent pyrolysis and gasification char prepared in the entrained flow reactor. *Fuel* **2019**, *240*, 126–137. [CrossRef]
47. Gollakota, A.; Kishore, N.; Gu, S. A review on hydrothermal liquefaction of biomass. *Renew. Sustain. Energy Rev.* **2018**, *81*, 1378–1392. [CrossRef]
48. Ponnusamy, V.K.; Nagappan, S.; Bhosale, R.R.; Lay, C.-H.; Nguyen, D.D.; Pugazhendhi, A.; Chang, S.W.; Kumar, G. Review on sustainable production of biochar through hydrothermal liquefaction: Physico-chemical properties and applications. *Bioresour. Technol.* **2020**, *310*, 123414. [CrossRef]
49. Abbas, A.; Mariana, L.T.; Phan, A.N. Biomass-waste derived graphene quantum dots and their applications. *Carbon* **2018**, *140*, 77–99. [CrossRef]
50. Wang, Q.; Liu, X.; Zhang, L.; Lv, Y. Microwave-assisted synthesis of carbon nanodots through an eggshell membrane and their fluorescent application. *Analyst* **2012**, *137*, 5392–5397. [CrossRef]
51. Xue, M.; Zou, M.; Zhao, J.; Zhan, Z.; Zhao, S. Green preparation of fluorescent carbon dots from lychee seeds and their application for the selective detection of methylene blue and imaging in living cells. *J. Mater. Chem. B* **2015**, *3*, 6783–6789. [CrossRef] [PubMed]
52. Zhou, Y.; Mintz, K.J.; Sharma, S.K.; Leblanc, R.M. Carbon dots: Diverse preparation, application, and perspective in surface chemistry. *Langmuir* **2019**, *35*, 9115–9132. [CrossRef] [PubMed]
53. Hsu, P.-C.; Shih, Z.-Y.; Lee, C.-H.; Chang, H.-T. Synthesis and analytical applications of photoluminescent carbon nanodots. *Green Chem.* **2012**, *14*, 917–920. [CrossRef]
54. Liu, S.; Tian, J.; Wang, L.; Zhang, Y.; Qin, X.; Luo, Y.; Asiri, A.M.; Al-Youbi, A.O.; Sun, X. Hydrothermal treatment of grass: A low-cost, green route to nitrogen-doped, carbon-rich, photoluminescent polymer nanodots as an effective fluorescent sensing platform for label-free detection of Cu (II) ions. *Adv. Mater.* **2012**, *24*, 2037–2041. [CrossRef] [PubMed]
55. Zhou, J.; Sheng, Z.; Han, H.; Zou, M.; Li, C. Facile synthesis of fluorescent carbon dots using watermelon peel as a carbon source. *Mater. Lett.* **2012**, *66*, 222–224. [CrossRef]
56. Zhou, S.; Sui, Y.; Zhu, X.; Sun, X.; Zhuo, S.; Li, H. Study and Comparison on Purification Methods of Multicolor Emission Carbon Dots. *Chem. –Asian J.* **2021**, *16*, 348–354. [CrossRef] [PubMed]
57. Zhou, Y.; Liyanage, P.Y.; Geleroff, D.L.; Peng, Z.; Mintz, K.J.; Hettiarachchi, S.D.; Pandey, R.R.; Chusuei, C.C.; Blackwelder, P.L.; Leblanc, R.M. Photoluminescent Carbon Dots: A Mixture of Heterogeneous Fractions. *ChemPhysChem* **2018**, *19*, 2589–2597. [CrossRef] [PubMed]
58. Zhou, Y.; Zahran, E.M.; Quiroga, B.A.; Perez, J.; Mintz, K.J.; Peng, Z.; Liyanage, P.Y.; Pandey, R.R.; Chusuei, C.C.; Leblanc, R.M. Size-dependent photocatalytic activity of carbon dots with surface-state determined photoluminescence. *Appl. Catal. B Environ.* **2019**, *248*, 157–166. [CrossRef] [PubMed]
59. da Silva, J.C.E.; Gonçalves, H.M. Analytical and bioanalytical applications of carbon dots. *TrAC Trends Anal. Chem.* **2011**, *30*, 1327–1336. [CrossRef]
60. Zhu, L.; Shen, D.; Wu, C.; Gu, S. State-of-the-Art on the Preparation, Modification, and Application of Biomass-Derived Carbon Quantum Dots. *Ind. Eng. Chem. Res.* **2020**, *59*, 22017–22039. [CrossRef]
61. Zhu, S.; Song, Y.; Zhao, X.; Shao, J.; Zhang, J.; Yang, B. The photoluminescence mechanism in carbon dots (graphene quantum dots, carbon nanodots, and polymer dots): Current state and future perspective. *Nano Res.* **2015**, *8*, 355–381. [CrossRef]
62. Zhu, S.; Song, Y.; Wang, J.; Wan, H.; Zhang, Y.; Ning, Y.; Yang, B. Photoluminescence mechanism in graphene quantum dots: Quantum confinement effect and surface/edge state. *Nano Today* **2017**, *13*, 10–14. [CrossRef]
63. Lin, L.; Zhang, S. Creating high yield water soluble luminescent graphene quantum dots via exfoliating and disintegrating carbon nanotubes and graphite flakes. *Chem. Commun.* **2012**, *48*, 10177–10179. [CrossRef] [PubMed]
64. Song, Y.; Zhu, S.; Shao, J.; Yang, B. Polymer carbon dots—A highlight reviewing their unique structure, bright emission and probable photoluminescence mechanism. *J. Polym. Sci. Part A Polym. Chem.* **2017**, *55*, 610–615. [CrossRef]
65. Yu, J.; Liu, C.; Yuan, K.; Lu, Z.; Cheng, Y.; Li, L.; Zhang, X.; Jin, P.; Meng, F.; Liu, H. Luminescence Mechanism of Carbon Dots by Tailoring Functional Groups for Sensing Fe^{3+} Ions. *Nanomaterials* **2018**, *8*, 233. [CrossRef]
66. Zu, F.; Yan, F.; Bai, Z.; Xu, J.; Wang, Y.; Huang, Y.; Zhou, X. The quenching of the fluorescence of carbon dots: A review on mechanisms and applications. *Microchim. Acta* **2017**, *184*, 1899–1914. [CrossRef]
67. Hu, C.; Lin, T.-J.; Huang, Y.-C.; Chen, Y.-Y.; Wang, K.-H.; Lin, K.-Y.A. Photoluminescence quenching of thermally treated waste-derived carbon dots for selective metal ion sensing. *Environ. Res.* **2021**, *197*, 111008. [CrossRef] [PubMed]
68. Xiong, Y.; Schneider, J.; Ushakova, E.V.; Rogach, A.L. Influence of molecular fluorophores on the research field of chemically synthesized carbon dots. *Nano Today* **2018**, *23*, 124–139. [CrossRef]

69. Rajendran, S.; Ramanaiah, D.V.; Kundu, S.; Bhunia, S.K. Yellow Fluorescent Carbon Dots for Selective Recognition of As^{3+} and Fe^{3+} Ions. *ACS Appl. Nano Mater.* **2021**, *4*, 10931–10942. [CrossRef]

70. Lee, H.; Su, Y.-C.; Tang, H.-H.; Lee, Y.-S.; Lee, J.-Y.; Hu, C.-C.; Chiu, T.-C. One-pot hydrothermal synthesis of carbon dots as fluorescent probes for the determination of mercuric and hypochlorite ions. *Nanomaterials* **2021**, *11*, 1831. [CrossRef] [PubMed]

71. Fu, Y.; Huang, L.; Zhao, S.; Xing, X.; Lan, M.; Song, X. A carbon dot-based fluorometric probe for oxytetracyline detection utilizing a Förster resonance energy transfer mechanism. *Spectrochim. Acta Part A Mol. Biomol. Spectrosc.* **2021**, *246*, 118947. [CrossRef] [PubMed]

72. Wang, L.; Jana, J.; Chung, J.S.; Hur, S.H. Glutathione modified N-doped carbon dots for sensitive and selective dopamine detection. *Dye. Pigment.* **2021**, *186*, 109028. [CrossRef]

73. Liu, S.; Zhao, N.; Cheng, Z.; Liu, H. Amino-functionalized green fluorescent carbon dots as surface energy transfer biosensors for hyaluronidase. *Nanoscale* **2015**, *7*, 6836–6842. [CrossRef] [PubMed]

74. Zhang, H.; Liu, J.; Wang, B.; Liu, K.; Chen, G.; Yu, X.; Li, J.; Yu, J. Zeolite-confined carbon dots: Tuning thermally activated delayed fluorescence emission via energy transfer. *Mater. Chem. Front.* **2020**, *4*, 1404–1410. [CrossRef]

75. Li, G.; Fu, H.; Chen, X.; Gong, P.; Chen, G.; Xia, L.; Wang, H.; You, J.; Wu, Y. Facile and sensitive fluorescence sensing of alkaline phosphatase activity with photoluminescent carbon dots based on inner filter effect. *Anal. Chem.* **2016**, *88*, 2720–2726. [CrossRef] [PubMed]

76. Fraiji, L.K.; Hayes, D.M.; Werner, T. Static and dynamic fluorescence quenching experiments for the physical chemistry laboratory. *J. Chem. Educ.* **1992**, *69*, 424. [CrossRef]

77. Sahoo, H. Förster resonance energy transfer—A spectroscopic nanoruler: Principle and applications. *J. Photochem. Photobiol. C Photochem. Rev.* **2011**, *12*, 20–30. [CrossRef]

78. Doose, S.; Neuweiler, H.; Sauer, M. Fluorescence Quenching by Photoinduced Electron Transfer: A Reporter for Conformational Dynamics of Macromolecules. *ChemPhysChem* **2009**, *10*, 1389–1398. [CrossRef]

79. Vaishnav, J.K.; Mukherjee, T.K. Long-range resonance coupling-induced surface energy transfer from CdTe quantum dot to plasmonic nanoparticle. *J. Phys. Chem. C* **2018**, *122*, 28324–28336. [CrossRef]

80. Amjadi, M.; Abolghasemi-Fakhri, Z.; Hallaj, T. Carbon dots-silver nanoparticles fluorescence resonance energy transfer system as a novel turn-on fluorescent probe for selective determination of cysteine. *J. Photochem. Photobiol. A Chem.* **2015**, *309*, 8–14. [CrossRef]

81. Guillet, J. *Polymer Photophysics and Photochemistry*; John Wiley & Sons: New York, NY, USA, 2010.

82. Chen, S.; Yu, Y.-L.; Wang, J.-H. Inner filter effect-based fluorescent sensing systems: A review. *Anal. Chim. Acta* **2018**, *999*, 13–26. [CrossRef]

83. Bhattacharjee, L.; Manoharan, R.; Mohanta, K.; Bhattacharjee, R.R. Conducting carbon quantum dots–a nascent nanomaterial. *J. Mater. Chem. A* **2015**, *3*, 1580–1586. [CrossRef]

84. Spanu, D.; Binda, G.; Dossi, C.; Monticelli, D. Biochar as an alternative sustainable platform for sensing applications: A review. *Microchem. J.* **2020**, *159*, 105506. [CrossRef]

85. Das, M.; Thakkar, H.; Patel, D.; Thakore, S. Repurposing the domestic organic waste into green emissive carbon dots and carbonized adsorbent: A sustainable zero waste process for metal sensing and dye sequestration. *J. Environ. Chem. Eng.* **2021**, *9*, 106312. [CrossRef]

86. Ding, S.; Gao, Y.; Ni, B.; Yang, X. Green synthesis of biomass-derived carbon quantum dots as fluorescent probe for Fe^{3+} detection. *Inorg. Chem. Commun.* **2021**, *130*, 108636. [CrossRef]

87. Jiao, X.-Y.; Li, L.-s.; Qin, S.; Zhang, Y.; Huang, K.; Xu, L. The synthesis of fluorescent carbon dots from mango peel and their multiple applications. *Colloids Surf. A Physicochem. Eng. Asp.* **2019**, *577*, 306–314. [CrossRef]

88. Shen, J.; Shang, S.; Chen, X.; Wang, D.; Cai, Y. Facile synthesis of fluorescence carbon dots from sweet potato for Fe^{3+} sensing and cell imaging. *Mater. Sci. Eng. C* **2017**, *76*, 856–864. [CrossRef] [PubMed]

89. Wang, C.; Shi, H.; Yang, M.; Yan, Y.; Liu, E.; Ji, Z.; Fan, J. Facile synthesis of novel carbon quantum dots from biomass waste for highly sensitive detection of iron ions. *Mater. Res. Bull.* **2020**, *124*, 110730. [CrossRef]

90. Sun, X.; He, J.; Yang, S.; Zheng, M.; Wang, Y.; Ma, S.; Zheng, H. Green synthesis of carbon dots originated from Lycii Fructus for effective fluorescent sensing of ferric ion and multicolor cell imaging. *J. Photochem. Photobiol. B Biol.* **2017**, *175*, 219–225. [CrossRef] [PubMed]

91. Zhu, L.; Shen, D.; Liu, Q.; Wu, C.; Gu, S. Sustainable synthesis of bright green fluorescent carbon quantum dots from lignin for highly sensitive detection of Fe^{3+} ions. *Appl. Surf. Sci.* **2021**, *565*, 150526. [CrossRef]

92. Qi, H.; Teng, M.; Liu, M.; Liu, S.; Li, J.; Yu, H.; Teng, C.; Huang, Z.; Liu, H.; Shao, Q.; et al. Biomass-derived nitrogen-doped carbon quantum dots: Highly selective fluorescent probe for detecting Fe^{3+} ions and tetracyclines. *J. Colloid Interface Sci.* **2019**, *539*, 332–341. [CrossRef]

93. Ahn, J.; Song, Y.; Kwon, J.E.; Lee, S.H.; Park, K.S.; Kim, S.; Woo, J.; Kim, H. Food waste-driven N-doped carbon dots: Applications for Fe^{3+} sensing and cell imaging. *Mater. Sci. Eng. C* **2019**, *102*, 106–112. [CrossRef]

94. Atchudan, R.; Edison, T.N.J.I.; Chakradhar, D.; Perumal, S.; Shim, J.-J.; Lee, Y.R. Facile green synthesis of nitrogen-doped carbon dots using Chionanthus retusus fruit extract and investigation of their suitability for metal ion sensing and biological applications. *Sens. Actuators B Chem.* **2017**, *246*, 497–509. [CrossRef]

95. Krishnaiah, P.; Atchudan, R.; Perumal, S.; Salama, E.-S.; Lee, Y.R.; Jeon, B.-H. Utilization of waste biomass of Poa pratensis for green synthesis of n-doped carbon dots and its application in detection of Mn^{2+} and Fe^{3+}. *Chemosphere* **2022**, *286*, 131764. [CrossRef]

96. Liu, Y.; Zhao, Y.; Zhang, Y. One-step green synthesized fluorescent carbon nanodots from bamboo leaves for copper(II) ion detection. *Sens. Actuators B Chem.* **2014**, *196*, 647–652. [CrossRef]

97. Bhamore, J.R.; Jha, S.; Park, T.J.; Kailasa, S.K. Fluorescence sensing of Cu^{2+} ion and imaging of fungal cell by ultra-small fluorescent carbon dots derived from Acacia concinna seeds. *Sens. Actuators B Chem.* **2018**, *277*, 47–54. [CrossRef]

98. Kamarol Zaman, A.S.; Tan, T.L.; A/P Chowmasundaram, Y.; Jamaludin, N.; Sadrolhosseini, A.R.; Rashid, U.; Rashid, S.A. Properties and molecular structure of carbon quantum dots derived from empty fruit bunch biochar using a facile microwave-assisted method for the detection of Cu^{2+} ions. *Opt. Mater.* **2021**, *112*, 110801. [CrossRef]

99. Gedda, G.; Lee, C.-Y.; Lin, Y.-C.; Wu, H.-f. Green synthesis of carbon dots from prawn shells for highly selective and sensitive detection of copper ions. *Sens. Actuators B Chem.* **2016**, *224*, 396–403. [CrossRef]

100. Bhamore, J.R.; Jha, S.; Singhal, R.K.; Park, T.J.; Kailasa, S.K. Facile green synthesis of carbon dots from Pyrus pyrifolia fruit for assaying of Al^{3+} ion via chelation enhanced fluorescence mechanism. *J. Mol. Liq.* **2018**, *264*, 9–16. [CrossRef]

101. Rao, H.; Liu, W.; He, K.; Zhao, S.; Lu, Z.; Zhang, S.; Sun, M.; Zou, P.; Wang, X.; Zhao, Q.; et al. Smartphone-Based Fluorescence Detection of Al^{3+} and H_2O Based on the Use of Dual-Emission Biomass Carbon Dots. *ACS Sustain. Chem. Eng.* **2020**, *8*, 8857–8867. [CrossRef]

102. Baragau, I.-A.; Power, N.P.; Morgan, D.J.; Lobo, R.A.; Roberts, C.S.; Titirici, M.-M.; Middelkoop, V.; Diaz, A.; Dunn, S.; Kellici, S. Efficient Continuous Hydrothermal Flow Synthesis of Carbon Quantum Dots from a Targeted Biomass Precursor for On–Off Metal Ions Nanosensing. *ACS Sustain. Chem. Eng.* **2021**, *9*, 2559–2569. [CrossRef]

103. Gu, D.; Shang, S.; Yu, Q.; Shen, J. Green synthesis of nitrogen-doped carbon dots from lotus root for Hg(II) ions detection and cell imaging. *Appl. Surf. Sci.* **2016**, *390*, 38–42. [CrossRef]

104. Li, Z.; Zhang, Y.; Niu, Q.; Mou, M.; Wu, Y.; Liu, X.; Yan, Z.; Liao, S. A fluorescence probe based on the nitrogen-doped carbon dots prepared from orange juice for detecting Hg^{2+} in water. *J. Lumin.* **2017**, *187*, 274–280. [CrossRef]

105. Xiong, Z.; Zou, Y.; Cao, X.; Lin, Z. Color-Tunable Fluorescent Nitrogen-doped Graphene Quantum Dots Derived from Pineapple Leaf Fiber Biomass to detect Hg^{2+}. *Chin. J. Anal. Chem.* **2022**, *50*, 69–76. [CrossRef]

106. Ye, Q.; Yan, F.; Luo, Y.; Wang, Y.; Zhou, X.; Chen, L. Formation of N, S-codoped fluorescent carbon dots from biomass and their application for the selective detection of mercury and iron ion. *Spectrochim. Acta Part A Mol. Biomol. Spectrosc.* **2017**, *173*, 854–862. [CrossRef]

107. Lu, H.; Li, C.; Wang, H.; Wang, X.; Xu, S. Biomass-Derived Sulfur, Nitrogen Co-Doped Carbon Dots for Colorimetric and Fluorescent Dual Mode Detection of Silver (I) and Cell Imaging. *ACS Omega* **2019**, *4*, 21500–21508. [CrossRef] [PubMed]

108. Zhao, X.; Liao, S.; Wang, L.; Liu, Q.; Chen, X. Facile green and one-pot synthesis of purple perilla derived carbon quantum dot as a fluorescent sensor for silver ion. *Talanta* **2019**, *201*, 1–8. [CrossRef] [PubMed]

109. Ramezani, Z.; Qorbanpour, M.; Rahbar, N. Green synthesis of carbon quantum dots using quince fruit (Cydonia oblonga) powder as carbon precursor: Application in cell imaging and As^{3+} determination. *Colloids Surf. A Physicochem. Eng. Asp.* **2018**, *549*, 58–66. [CrossRef]

110. Zhao, C.; Li, X.; Cheng, C.; Yang, Y. Green and microwave-assisted synthesis of carbon dots and application for visual detection of cobalt(II) ions and pH sensing. *Microchem. J.* **2019**, *147*, 183–190. [CrossRef]

111. Chellasamy, G.; Arumugasamy, S.K.; Govindaraju, S.; Yun, K. Green synthesized carbon quantum dots from maple tree leaves for biosensing of Cesium and electrocatalytic oxidation of glycerol. *Chemosphere* **2022**, *287*, 131915. [CrossRef]

112. Yin, B.; Deng, J.; Peng, X.; Long, Q.; Zhao, J.; Lu, Q.; Chen, Q.; Li, H.; Tang, H.; Zhang, Y. Green synthesis of carbon dots with down-and up-conversion fluorescent properties for sensitive detection of hypochlorite with a dual-readout assay. *Analyst* **2013**, *138*, 6551–6557. [CrossRef] [PubMed]

113. Jin, H.; Gui, R.; Wang, Y.; Sun, J. Carrot-derived carbon dots modified with polyethyleneimine and nile blue for ratiometric two-photon fluorescence turn-on sensing of sulfide anion in biological fluids. *Talanta* **2017**, *169*, 141–148. [CrossRef] [PubMed]

114. Boruah, A.; Saikia, M.; Das, T.; Goswamee, R.L.; Saikia, B.K. Blue-emitting fluorescent carbon quantum dots from waste biomass sources and their application in fluoride ion detection in water. *J. Photochem. Photobiol. B Biol.* **2020**, *209*, 111940. [CrossRef]

115. Ofir, E.; Oren, Y.; Adin, A. Comparing pretreatment by iron of electro-flocculation and chemical flocculation. *Desalination* **2007**, *204*, 87–93. [CrossRef]

116. Şenol, A.M.; Onganer, Y. A novel "turn-off" fluorescent sensor based on cranberry derived carbon dots to detect iron (III) and hypochlorite ions. *J. Photochem. Photobiol. A Chem.* **2022**, *424*, 113655. [CrossRef]

117. Liu, X.; Xu, Z.; Cole, J.M. Molecular Design of UV–vis Absorption and Emission Properties in Organic Fluorophores: Toward Larger Bathochromic Shifts, Enhanced Molar Extinction Coefficients, and Greater Stokes Shifts. *J. Phys. Chem. C* **2013**, *117*, 16584–16595. [CrossRef]

118. Araneda, J.F.; Piers, W.E.; Heyne, B.; Parvez, M.; McDonald, R. High Stokes Shift Anilido-Pyridine Boron Difluoride Dyes. *Angew. Chem. Int. Ed.* **2011**, *50*, 12214–12217. [CrossRef]

119. Malhotra, N.; Ger, T.-R.; Uapipatanakul, B.; Huang, J.-C.; Chen, K.H.-C.; Hsiao, C.-D. Review of copper and copper nanoparticle toxicity in fish. *Nanomaterials* **2020**, *10*, 1126. [CrossRef]

120. Schanz, F.R.; Sommer, S.; Lami, A.; Fontaneto, D.; Ozgul, A. Life-history responses of a freshwater rotifer to copper pollution. *Ecol. Evol.* **2021**, *11*, 10947–10955. [CrossRef] [PubMed]

121. Taylor, A.A.; Tsuji, J.S.; Garry, M.R.; McArdle, M.E.; Goodfellow, W.L.; Adams, W.J.; Menzie, C.A. Critical review of exposure and effects: Implications for setting regulatory health criteria for ingested copper. *Environ. Manag.* **2020**, *65*, 131–159. [CrossRef] [PubMed]

122. Yokel, R.A. The toxicology of aluminum in the brain: A review. *Neurotoxicology* **2000**, *21*, 813–828.

123. Bernhoft, R.A. Mercury toxicity and treatment: A review of the literature. *J. Environ. Public Health* **2012**, *2012*, 460508. [CrossRef] [PubMed]

124. Liu, Z.; Jin, W.; Wang, F.; Li, T.; Nie, J.; Xiao, W.; Zhang, Q.; Zhang, Y. Ratiometric fluorescent sensing of Pb^{2+} and Hg^{2+} with two types of carbon dot nanohybrids synthesized from the same biomass. *Sens. Actuators B Chem.* **2019**, *296*, 126698. [CrossRef]

125. Fu, L.; Liu, T.; Yang, F.; Wu, M.; Yin, C.; Chen, L.; Niu, N. A multi-channel array for metal ions discrimination with animal bones derived biomass carbon dots as sensing units. *J. Photochem. Photobiol. A Chem.* **2022**, *424*, 113638. [CrossRef]

126. Plácido, J.; Bustamante-López, S.; Meissner, K.E.; Kelly, D.E.; Kelly, S.L. Microalgae biochar-derived carbon dots and their application in heavy metal sensing in aqueous systems. *Sci. Total Environ.* **2019**, *656*, 531–539. [CrossRef]

127. Guo, Y.; Yang, L.; Li, W.; Wang, X.; Shang, Y.; Li, B. Carbon dots doped with nitrogen and sulfur and loaded with copper (II) as a "turn-on" fluorescent probe for cystein, glutathione and homocysteine. *Microchim. Acta* **2016**, *183*, 1409–1416. [CrossRef]

128. Ensafi, A.A.; Hghighat Sefat, S.; Kazemifard, N.; Rezaei, B.; Moradi, F. A novel one-step and green synthesis of highly fluorescent carbon dots from saffron for cell imaging and sensing of prilocaine. *Sens. Actuators B Chem.* **2017**, *253*, 451–460. [CrossRef]

129. Liu, H.; Ding, J.; Chen, L.; Ding, L. A novel fluorescence assay based on self-doping biomass carbon dots for rapid detection of dimethoate. *J. Photochem. Photobiol. A Chem.* **2020**, *400*, 112724. [CrossRef]

130. Yan, Z.; Zhang, Z.; Chen, J. Biomass-based carbon dots: Synthesis and application in imatinib determination. *Sens. Actuators B Chem.* **2016**, *225*, 469–473. [CrossRef]

131. Wang, L.; Bi, Y.; Hou, J.; Li, H.; Xu, Y.; Wang, B.; Ding, H.; Ding, L. Facile, green and clean one-step synthesis of carbon dots from wool: Application as a sensor for glyphosate detection based on the inner filter effect. *Talanta* **2016**, *160*, 268–275. [CrossRef]

132. Lu, X.; Liu, C.; Wang, Z.; Yang, J.; Xu, M.; Dong, J.; Wang, P.; Gu, J.; Cao, F. Nitrogen-doped carbon nanoparticles derived from silkworm excrement as on–off–on fluorescent sensors to detect Fe (III) and biothiols. *Nanomaterials* **2018**, *8*, 443. [CrossRef] [PubMed]

133. Fan, P.; Liu, C.; Hu, C.; Li, F.; Lin, X.; Yang, S.; Xiao, F. Green and facile synthesis of biomass iron-doped carbon dots as dual-signal colorimetric and fluorometric probe for the detection of ascorbic acid. *New J. Chem.* **2022**, *46*, 2526–2533. [CrossRef]

134. Zheng, M.; Wang, C.; Wang, Y.; Wei, W.; Ma, S.; Sun, X.; He, J. Green synthesis of carbon dots functionalized silver nanoparticles for the colorimetric detection of phoxim. *Talanta* **2018**, *185*, 309–315. [CrossRef] [PubMed]

135. Tang, X.; Wang, H.; Yu, H.; Bui, B.; Zhang, W.; Wang, S.; Chen, M.; Yuan, L.; Hu, Z.; Chen, W. Exploration of nitrogen-doped grape peels carbon dots for baicalin detection. *Mater. Today Phys.* **2022**, *22*, 100576. [CrossRef]

136. Liang, Y.-M.; Yang, H.; Zhou, B.; Chen, Y.; Yang, M.; Wei, K.-S.; Yan, X.-F.; Kang, C. Waste tobacco leaves derived carbon dots for tetracycline detection: Improving quantitative accuracy with the aid of chemometric model. *Anal. Chim. Acta* **2021**, *1191*, 339269. [CrossRef] [PubMed]

137. Liu, H.; Ding, L.; Chen, L.; Chen, Y.; Zhou, T.; Li, H.; Xu, Y.; Zhao, L.; Huang, N. A facile, green synthesis of biomass carbon dots coupled with molecularly imprinted polymers for highly selective detection of oxytetracycline. *J. Ind. Eng. Chem.* **2019**, *69*, 455–463. [CrossRef]

138. Miao, H.; Wang, Y.; Yang, X. Carbon dots derived from tobacco for visually distinguishing and detecting three kinds of tetracyclines. *Nanoscale* **2018**, *10*, 8139–8145. [CrossRef] [PubMed]

139. Tang, X.; Wang, L.; Ye, H.; Zhao, H.; Zhao, L. Biological matrix-derived carbon quantum dots: Highly selective detection of tetracyclines. *J. Photochem. Photobiol. A Chem.* **2022**, *424*, 113653. [CrossRef]

140. Deblonde, T.; Cossu-Leguille, C.; Hartemann, P. Emerging pollutants in wastewater: A review of the literature. *Int. J. Hyg. Environ. Health* **2011**, *214*, 442–448. [CrossRef] [PubMed]

141. Saleh, H.; Elhenawee, M.; Hussien, E.M.; Ahmed, N.; Ibrahim, A.E. Validation of hplc-uv multi-residue method for the simultaneous determination of tetracycline, oxytetracycline, spiramycin and neospiramycin in raw milk. *Food Anal. Methods* **2021**, *14*, 36–43. [CrossRef]

142. Gunjal, D.B.; Gurav, Y.M.; Gore, A.H.; Naik, V.M.; Waghmare, R.D.; Patil, C.S.; Sohn, D.; Anbhule, P.V.; Shejwal, R.V.; Kolekar, G.B. Nitrogen doped waste tea residue derived carbon dots for selective quantification of tetracycline in urine and pharmaceutical samples and yeast cell imaging application. *Opt. Mater.* **2019**, *98*, 109484. [CrossRef]

143. Farshbaf, M.; Davaran, S.; Rahimi, F.; Annabi, N.; Salehi, R.; Akbarzadeh, A. Carbon quantum dots: Recent progresses on synthesis, surface modification and applications. *Artif. Cells Nanomed. Biotechnol.* **2018**, *46*, 1331–1348. [CrossRef] [PubMed]

144. Das, R.; Bandyopadhyay, R.; Pramanik, P. Carbon quantum dots from natural resource: A review. *Mater. Today Chem.* **2018**, *8*, 96–109. [CrossRef]

145. Molaei, M.J. Principles, mechanisms, and application of carbon quantum dots in sensors: A review. *Anal. Methods* **2020**, *12*, 1266–1287. [CrossRef]